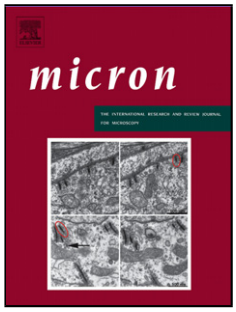

Title: Electron Scattering Cross Section Measurements in a Variable Pressure Scanning Electron Microscope

Authors: Scott A. Wight, Andrew R. Konicek

PII: S0968-4328(12)00112-6
DOI: doi:10.1016/j.micron.2012.04.003
Reference: JMIC 1812

To appear in: *Micron*

Received date: 10-1-2012
Revised date: 5-4-2012
Accepted date: 5-4-2012

Please cite this article as: Wight, S.A., Konicek, A.R., Electron Scattering Cross Section Measurements in a Variable Pressure Scanning Electron Microscope, *Micron* (2010), doi:10.1016/j.micron.2012.04.003

Title: Electron Scattering Cross Section Measurements in a Variable Pressure Scanning Electron Microscope

Author Names and Affiliations:

Scott A. Wight and Andrew R. Konicek

Surface and Microanalysis Science Division
National Institute of Standards and Technology
100 Bureau Drive, Stop 8371
Gaithersburg, MD 20899 USA

Abstract

Scattering of the incident electron beam in the variable pressure scanning electron microscope (VPSEM) affects the ability to perform quantitative chemical measurements. However, the manner in which the sum of the elastic and inelastic scattering cross sections varies as a function of gas type and accelerating voltage in the VPSEM is not well understood. A dual Faraday cup was constructed to measure the scattered fraction of the primary beam as a function of gas pressure, working distance, and accelerating voltage in air, water vapor, and argon environments. Experimentally measured values of the scattering cross section agree with previous experimental work, and agree within a factor of two with those values calculated carefully from theory.

Keywords: scattering cross section; stagnation gas thickness; beam gas path length; electron scattering; environmental scanning electron microscope; ESEM; VPSEM.

Running Title: Scattering Cross Section Measurements

Corresponding Author: Scott Wight, scott.wight@nist.gov, +1(301) 975-3949

Introduction

The controlled introduction of gas into the specimen chamber has created a new class of scanning electron microscope (SEM). Names such as variable pressure, low vacuum, environmental, nature, wet, atmospheric, and even leaky vacuum, are used to describe these unconventional SEMs. For the purposes of this manuscript, we will refer to them generically as variable pressure scanning electron microscopes (VPSEM). The presence of a gas provides charge carriers that can facilitate specimen charge neutralization under electron bombardment, reduce the evaporation rate of wet specimens, or even, in some situations, maintain the specimen in a wet state during electron beam interrogation. The downside is that gas molecules scatter electrons out of the primary beam as it travels through the specimen chamber. The scattering cross section (σ) is a measure of the magnitude of the electron scattering that occurs above the specimen surface.

Electroscan Corporation[1] introduced the first commercial environmental SEM or ESEM™ in 1988 based upon the work of Danilatos who, in the same year, published the seminal "Foundations" paper (Danilatos, 1988). Danilatos discussed in detail issues concerning electron scattering in the gas, the creation of an electron "skirt" on the specimen, and the calculation of σ, and continues to make significant contributions to the field (Danilatos, 2012). Several authors

[1] Certain commercial equipment, instruments, or materials are identified in this report to specify adequately the experimental procedure. Such identification does not imply recommendation or endorsement by the National Institute of Standards and Technology, nor does it imply that the materials or equipment identified are necessarily the best available for the purpose.

(Griffin, 1992, Carlton, 1997, Wight *et al*., 1997, Stowe and Robinson, 1998, Wight and Zeissler, 2000, Gauvin *et al*., 2002, Wight, 2001, He and Joy, 2002, He and Joy, 2003, Kadoun*, et al*., 2003, Belkorissat, *et al*., 2004, Mathieu, *et al*., 2007, Rattenberger *et al.*, 2009, Danilatos, et al., 2010) have made experimental measurements of electron scattering in the VPSEM and a few (Bolon, 1991, Griffin and Nockolds, 1996, Horsewell, *et al*., 1996, Bilde-Sorensen and Appel, 1997, Doehne, 1997, Mansfield, 2000, Newbury, 2002, Griffin and Suvorova, 2003, Khouchaf, *et al*., 2010) have suggested schemes to correct for spurious x-rays generated by scattered electrons during x-ray microanalysis performed in the VPSEM. Much of the previous experimental work does not apply to modern field emission gun instruments with shorter working distances.

We were in part motivated by Rattenberger and coworkers (Rattenberger *et al.*, 2009), who created a dual Faraday cup and used it to experimentally determine the beam gas path length (BGPL) and σ for nitrogen, air, and water vapor, in a field emission gun SEM, focusing on pressures between 40 Pa and 130 Pa. This pressure range is limited compared to the range of pressures available in a commercial VPSEM.

This paper aims to expand upon the previous work by measuring the unscattered beam current using a dual Faraday cup device in a field emission gun instrument and a broader range of gas pressures. A dual Faraday cup was fabricated with a similar design to that described in the Rattenberger paper (2009), but with a smaller diameter aperture. This smaller top aperture is more effective at separating the scattered electrons from the primary beam electrons. We focus on gaining understanding of electron scattering as it is affected by gas type, gas pressure, and also the voltage applied to the gaseous secondary electron detector (GSED). The tested gas pressures, 27 Pa to 665 Pa (0.2 Torr to 5.0 Torr), cover the practical range of pressures used

routinely in VPSEM. An experimental confirmation of the calculated theoretical σ will allow for better prediction of scattering for future experiments. Concise documentation of the experimental procedure is included here for any future researcher who might want to compare results from another VPSEM or at additional operating conditions.

Materials and Methods

The core of the dual Faraday cup is a 12 mm diameter by 10 mm high graphite cylinder (Fig. 1). Graphite was chosen for its good electrical conductivity, and, most importantly, its low backscatter yield. Backscattered electrons that escape out of the Faraday cup will reduce the accuracy of the measured cup current, leading to an overestimation of the σ of each gas species. To further reduce the likelihood of electrons escaping the cup, thereby increasing the collection efficiency, the 1 mm diameter hole in the center of the graphite was drilled at roughly a 10 degree angle from the surface normal such that the bottom of the hole is not aligned with the top of the hole when viewed from the surface normal. The center conductor of a shielded BNC cable was connected with carbon paint to a hole in the side of the graphite matching the diameter of the conductor. The graphite block, with the exception of the top surface, was embedded in a 25 mm diameter epoxy block for stability and electrical isolation. Next, a 200 micrometer diameter aperture was positioned over the center of the 1 mm hole in the graphite. This inner aperture was fixed in place with carbon paint, which also provides an electrical contact to the graphite. The top surface of the epoxy/graphite/aperture was then covered with double stick tape. A layer of 6 micrometer thick Mylar was placed over the tape, and then another layer of double stick tape was placed orthogonal to the original layer. The tape serves two functions: it is both an electrical

insulator, and it holds the layers in place. Under an inspection scope, a 0.5 mm × 0.5 mm square of tape was cut away to reveal the 200 micrometer aperture. A piece of 6 micrometer thick nickel foil was cut large enough to completely cover the epoxy surface. A 1 mm × 1 mm hole was cut with a scalpel in the center of the nickel foil. Under the inspection scope, the foil was placed on the tape such that the 200 micrometer aperture was aligned to the center of the opening in the foil. Finally, using a light microscope with a cross-hair reticule, a 5 micrometer diameter platinum aperture was aligned with the 200 micrometer aperture and then held in place with carbon paint. The center conductor of a second shielded BNC cable was silver painted to the tab on the nickel foil, and then glued in place for stability. The device was tested to ensure there was no electrical continuity between the buried cup and the top surface.

The SEM used in this work was a FEI Company (Hillsboro, OR) ESEM. The ESEM model number is a Quanta 200F and it has a thermally assisted field emission gun. The microscope operates in 3 vacuum modes: 1) high vacuum of 10^{-2} Pa to 10^{-4} Pa (10^{-4} Torr to 10^{-6} Torr), which is similar to any conventional SEM, 2) low vacuum, where up to 133 Pa (1 Torr) of gas (usually water vapor, but any lecture bottle can be connected) can be introduced to eliminate charging for insulating specimens, and 3) ESEM mode, where the gas pressure can be raised up to 3990 Pa (30 Torr) and is useful for either maintaining the hydration of wet specimens or dynamic hydration studies. ESEM mode was utilized for the data collection in this work because it provided access to a larger range of specimen chamber pressures. This allowed for a large range of scattering conditions, but the primary electron beam was never completely scattered to the point of being un-measureable. The manufacturer's specification quotes a spatial resolution for secondary electron imaging of 2 nm at 30 kV regardless of vacuum mode.

Two types of experimental data were collected – the unscattered beam current as a function of working distance at a fixed accelerating voltage, gas type, and gas pressure; and the unscattered beam current as a function of gas pressure at a fixed gas type, accelerating voltage, and working distance. Primary beam currents for a given accelerating voltage were measured in high vacuum. High vacuum measurements, and data collected at a fixed working distance, were at a 10.0 mm working distance. Experimental data at variable pressures were collected in ESEM mode with a GSED, having a 500 micrometer diameter pressure limiting aperture, attached to the pole piece. The dual Faraday cup assembly was attached to a 25 mm stub mount holder which was clamped into a single pin mount stage. The buried cup and top surface of the dual Faraday cup were each connected to coaxial feedthroughs on the chamber wall by shielded cables with BNC style connectors. A Keithley model 6485 picoammeter was connected to the buried graphite cup to measure the unscattered electron beam current. The top surface was connected to ground. The model 6485 picoammeter has 0.4% accuracy. For these measurements, the gas pressure was set to 27 Pa, 53 Pa, 80 Pa, 106 Pa, 133 Pa, 266 Pa, 399 Pa, 532 Pa, and 655 Pa (0.2 Torr, 0.4 Torr, 0.6 Torr, 0.8 Torr. 1.0 Torr, 2.0 Torr, 3.0 Torr, 4.0 Torr, and 5.0 Torr) and the automated pressure control system was allowed to settle to better than 1% of the nominal value before taking each current reading. Measurements of the unscattered current collected as a function of working distance were performed at 4 mm, 7 mm, 10 mm, 13 mm, 16 mm, and 19 mm working distances. Accelerating voltage data were collected at 5 kV, 10 kV, 15 kV, 20 kV, 25 kV, and 30 kV with a spot size of 3.0 and a 30 micrometer projection aperture. Chamber gases were water, air, or argon.

Working distance (WD) is the nominal distance from the pole piece to the specimen as calculated from lens strength. This may be above or below the actual pressure limiting aperture

depending on how the instrument manufacturer chooses to calculate or calibrate. If we assume for arguments sake that it calculates to the horizontal line midway between the top surface of the aperture and the bottom surface of the aperture, then this number still does not represent the actual length of the path that the electron travels thru the gas on its way to the specimen because there is gas that extends above the aperture when the chamber pressure is above high vacuum. The difference between the affective top of that gas plume and the midline is the distance we call delta. We have chosen to adopt the Danilatos, et al, 2011 terminology and refer to the WD plus the delta as "stagnation gas thickness" (SGT) or theta symbol.

Scattering cross sections were calculated from the measured current data using the unscattered current measurements as a function of working distance for fixed chamber pressures. Using Equation 1 (Danilatos, 1988, 2009),

$$I = I_0 \cdot e^{\frac{-\sigma p \cdot SGT}{k_B T}} = I_0 \cdot e^{-m} \qquad (1)$$

where I_0 is the total beam current (A) measured in high vacuum, I is the measured unscattered current (A), σ is the scattering cross section (meters^{-2}), p is the chamber pressure (Pa), SGT is the stagnation gas thickness (meters), k_B is the Boltzmann constant (1.38×10^{-23} J/K), and T is the gas temperature (K), the cup current measurements were normalized by the total beam current. The exponent value, m, the average number of collisions per electron, can then be calculated for each WD. However, a correction needs to be made to determine the SGT. Measurements in the VPSEM are performed with a known WD, which is close to but not equal to the SGT. Utilizing Equation 2, after measuring the current as a function of working distance, the data can be plotted as

$$m = \frac{\sigma \cdot p \cdot (WD + \Delta)}{k_B T} = (slope) \cdot (WD + \Delta) \quad (2)$$

where the slope in Equation 2 is determined by the scattering cross section, pressure, Boltzmann constant, and temperature. WD is the working distance (meters), and Δ is a microscope and gas pressure dependent length (meters). Examining Equation 2, if the SGT is zero there should be no electron collisions, meaning there should be a zero intercept. Therefore, Δ can be determined for each pressure using the slope from Equation 2, the fit parameter *m* from Equation 1, and the known working distances. At this point, the σ values can be calculated. All of the unscattered current measurements as a function of working distance at fixed pressures were done for the same electron accelerating voltage. The useful relationship is that of σ as a function of accelerating voltage. Data sets of unscattered current as a function of gas pressure were collected for a range of accelerating voltages. Assuming the SGT is constant for each gas type at each pressure, Equation 1 can be used to calculate the σ.

The theoretical calculations for the σ follow the equations in Danilatos (1988 and 1990), which have been used elsewhere (Rattenberger *et al.*, 2009, Kadoun, *et al*., 2003, Mansour *et al*., 2007), are included in the Appendix for completeness.

Results

Selected data for water, air, and argon at 133 Pa (1 Torr) and 20 kV accelerating voltage are plotted as the average number of collisions per electron versus SGT (Fig. 2a). Similarly, all pressures for water vapor are plotted as the average number of collisions per electron versus SGT (Fig. 2b) at 20 kV accelerating voltage. The measured σ along with the σ calculated for our experimental case with a 5 micrometer diameter aperture (which defines a minimum scattering angle of 2.5 x 10^{-4} rad.) are plotted for water (Fig. 3), air (Fig. 4), and argon (Fig. 5). The

theoretically calculated σ values in this work were calculated for our specific measurement geometry, and was done with both the first ionization potential (Danilatos, 1988), and the mean ionization potential (Mansour, *et al.*, 2010). Calculated σ for water, at several relevant minimum scattering angles are plotted as a function of accelerating voltage in Figure 6. The σ calculated from the dual Faraday cup measurements and uncertainties from propagating uncertainties (using the partial derivative method and reported with a coverage factor of 2) are compiled in Table 1, and Table 2 contains the parameters for power law fits to the measured σ versus accelerating voltage data.

Discussion

In the FEI Company VPSEM used in this work, the contrast setting on the secondary electron detector changes the bias applied to the detector, and thus the secondary electron cascade and consequently the excess of positive charge in the specimen chamber. For this reason, all measurements were conducted with the GSED contrast set to zero.

The construction of the dual Faraday cup allowed the measurement of the scattered current from the top surface of the device to be shunted to ground, allowing only the unscattered electron beam to be measured in the buried Faraday cup. As an example, each studied gas is plotted at 133 Pa as a function of the SGT to illustrate the effect of the different σ of each gas on the number of electron collisions (Figure 2a), where the SGT is independent of accelerating voltage. A linear relationship exists for each gas, with higher slopes for more strongly scattering gases. The offset of the SGT from the set WD, Δ, is similar between the different gases. The magnitude of the offset is dependent on the gas type and the dimensions of the pressure limiting aperture,

which is the GSED aperture in this experiment. Argon, with the highest σ, has a longer SGT for the same working distance compared to water, with the lowest σ. The SGT of air lies between those of water vapor and argon. The unscattered beam current data collected as a function of working distance for all pressures of water were utilized to calculate the average number of collisions per electron as a function of SGT (Figure 2b). Once again, a linear relationship exists for each gas pressure with the higher sloped lines corresponding to the higher pressures, where more scattering occurs. The data collected as a function of working distance has a much greater uncertainty at the shorter working distances than at the longer working distances. We estimate an error in the measured σ of up to 5% as a result of this experimental necessity. The Rattenberger (Rattenberger *et al.*, 2009) work is subject to the same limitation. The offset between the WD and the SGT in this set is variable as the pressure increases until the pressure goes above 133 Pa (1 Torr) where the offset becomes stable. There is a difference seen between the calculated σ values, using the experimental aperture size and working distance, and the experimentally determined σ values as a function of accelerating voltage for water vapor (Figure 3), air (Figure 4), and argon (Figure 5). Calculated values were made using both the first ionization potentials, as in Danilatos, 1988, and the mean ionization potentials, as in Mansour, *et al.*, 2010. The calculated values using the first ionization potentials differ with the experimental measurements within a factor of approximately two, and differ by a factor of 1.5 when using the mean ionization potentials. The limits of integration will affect the calculated values, and are not consistent between the previous works mentioned. Values for this manuscript were integrated from 2.5e-4 rad. to pi rad. for the elastic term, and from 2.5e-4 rad. to 0.17 rad. for the inelastic term. Danilatos, 1988, specifies the inelastic equations are only valid for angles less than 0.17 rad., but that the elastic equations are valid for all angles. The upper integration limit for the

inelastic term does not matter above 0.1 rad., as the elastic term dominates. Small changes to the high or low limit for the non-dominating term at those high or low angles do not have a substantial effect on the σ values. Error bars on the experimental data represent the cumulative uncertainty in the data collection that is propagated in subsequent calculations.

There is excellent agreement between the experimentally measured σ for water and air in this work and the measured values in (Rattenberger *et al.*, 2009). Our values are also within a factor of 2 of the experimental data taken by He and Joy (2003) for air, despite using a different experimental method. Their argon data agrees very well with ours for 10 kV, 15, kV, and 20 kV, but deviates at 25 kV and 30 kV. The experimental σ as a function of accelerating voltage data can be fit using a power law where the gas parameters A (m^2kV^{-1}) and B (dimensionless) are the multiplier and the exponent, respectively. Table 2 presents the gas parameters A and B for air, water vapor, and argon. Our calculated A and B for water are 1.573×10^{-20} and -0.905, respectively, and (Rattenberger *et al.*, 2009) reported 1.568×10^{-20} and -0.864. Likewise, for air, our 2.267×10^{-20} and -0.892 and (Rattenberger *et al.*, 2009) A and B for air are 2.475×10^{-20} and -0.904 exhibit good agreement. To better understand the small differences between our measured data for the σ and the theoretical values, additional calculations were made for the σ in water vapor using different effective aperture sizes. These calculations were performed using the mean ionization potentials. Each aperture and BGPL combination defines the minimum scattering angle necessary such that electrons deflected by more than that angle from the incident beam path would be blocked by the aperture in the experimental measurement. Plots of the σ as a function of voltage, assuming a 10 mm working distance, for a 20 nm aperture, a 5 μm aperture, a 10 μm aperture, a 20 μm aperture, and a 200 μm aperture, are displayed in Figure 6. There is little deviation, especially at 5 kV, between the calculated σ values for low minimum scattering

angles. In fact, the curves for the ideal case (minimum scattering angle of 1 x 10^{-6} rad.) and the aperture used in this paper (minimum scattering angle of 2.5 x 10^{-4} rad.) are very close over the entire 5 kV to 30 kV range. This suggests that, according to these equations, further scattering measurements can be made with a 5 μm top aperture which will effectively screen out nearly all scattered electrons. Surprisingly, the calculation for the 200 μm aperture (1 x 10^{-2} minimum scattering angle) is the best match for the experimental data. Note that the functional shape of the curve does not match the measured data, but the approximate magnitudes of the σ at all voltages are near the measured values.

Conclusions

The measured σ values in this work are in close agreement with those measured by other researchers for the same gases (He and Joy, 2003, Rattenberger *et al.*, 2009). The calculated σ values had good agreement with the measured values for the conditions used in this work. The σ calculations were higher by about a factor of two for all voltages and for all gases when using the first ionization potential, and about a factor of 1.5 when using the mean ionization potential. These results will be useful to microanalysts for calculating the amount of scattering the beam undergoes for their specific measurement conditions. It is important to note that σ values are not instrument specific, but are a function of the gas type and electron accelerating voltage. This scattering effect is even more important when performing chemical measurements with energy dispersive x-ray spectroscopy. The scattered incident electrons will create x-rays from regions of the sample outside of the incident beam path, convolving the chemical information from a larger area and thereby reducing the chemical resolution.

While our measured values for σ did not agree perfectly with the calculated values using the minimum scattering angle for a 5 μm aperture, the calculation did match very closely to the ideal calculation (minimum scattering angle of 10^{-6} rad.) that accounts for every electron that scatters outside the diameter of the starting beam. Assuming the general trend of the calculated values remains the same, and there is only a net shift that would accurately describe the true scattering behavior, then this would suggest that a 5 μm aperture is a satisfactory facsimile of the ideal aperture. Construction of this specialized type of Faraday cup is a critical component of these measurements. The 5 micrometer aperture is large enough to work with, but still small enough to screen most of the scattered electrons. Using graphite as a cup material, along with the cup hole being drilled at an angle, reduces losses from backscattered electrons.

Appendix

The σ is calculated by (Danilatos, 1988)

$$\sigma = 2 \cdot \pi \cdot \int_0^{\pi} \left(\frac{d\sigma_e}{d\Omega} + \frac{d\sigma_i}{d\Omega} \right) \cdot \sin(\theta) \cdot d\theta \tag{3}$$

where the sum in the integral is of the differential elastic cross section and the differential inelastic cross section, respectively, and it is integrated over all polar angles, θ, from the beam normal. The expression for the elastic differential cross section is

$$\left(\frac{d\sigma_e}{d\Omega} \right)_{Atomic} = \frac{A \cdot Z}{16 \cdot \left[\sin^2\left(\frac{\theta}{2}\right) + \sin^2\left(\frac{\theta_0}{2}\right) \right]^2} \tag{4}$$

and the expression for the inelastic differential cross section is

$$\left(\frac{d\sigma_i}{d\Omega} \right)_{Atomic} = \frac{A \cdot \left(\theta^2 + \theta_E^2 + 2 \cdot \theta_0^2\right)}{\left(\theta^2 + \theta_E^2\right) \cdot \left(\theta^2 + \theta_E^2 + \theta_0^2\right)^2} \tag{5}$$

where Z is the atomic number, and

$$A = \frac{\lambda^4 \cdot Z \cdot \left(1 + \frac{E}{E_0}\right)^2}{4 \cdot \pi^4 \cdot a_H^2} \tag{6}$$

$$\theta_0 = \frac{\lambda}{2 \cdot \pi \cdot R} \tag{7}$$

$$\theta_E = \frac{J}{4 \cdot E} \tag{8}$$

λ is the electron wavelength, calculated by

$$\lambda = 1.226 \cdot 10^{-9} \cdot \left[E \cdot \left(1 + 0.9778 \cdot 10^{-6} \cdot E\right) \right]^{-0.5} \tag{9}$$

where E is the electron energy (eV), E_0 is the electron rest mass (511,000 eV), a_H is the Bohr radius (5.29×10^{-11} m), J is taken as the first ionization potential (eV), and R is the atomic radius (m), calculated by

$$R = \left[f_e(0) \cdot \frac{a_H}{2 \cdot Z} \right]^{0.5} \quad (10)$$

where $f_e(0)$ is the scattering amplitude.

The equations for the atomic differential scattering cross sections are related to those for the molecular differential cross sections. The molecular contribution to the inelastic σ is calculated by the addition of all of the individual atomic differential inelastic cross sections, given in Equation 11

$$\left(\frac{d\sigma_i}{d\Omega}\right)_{Molecular} = \sum_x \left[\left(\frac{d\sigma_i}{d\Omega}\right)_{Atomic} \right]_x \quad (11)$$

as this type of scattering is incoherent. The molecular elastic differential cross section has both coherent and incoherent scattering, given as

$$\left(\frac{d\sigma_e}{d\Omega}\right)_{Molecular} = \sum_x \sum_y f_x(\theta) \cdot f_y(\theta) \cdot \frac{\sin(s \cdot r_{xy})}{s \cdot r_{xy}} \quad (12)$$

where the sums over *x* and *y* are both performed for all atoms in the molecule, and r_{xy} is the inter-atomic distance,

$$\left(\frac{d\sigma_e}{d\Omega}\right)_{Atomic} = |f_x(\theta)|^2 \quad (13)$$

is used to find the scattering amplitudes, $f_x(\theta)$, and

$$s = \frac{4 \cdot \pi \cdot \sin\left(\frac{\theta}{2}\right)}{\lambda} \quad (14)$$

where θ and λ are defined above. The elastic term, for the example of a diatomic molecule, will yield two sets of equal terms. Two will be for when x is equal to y, in which case the sine term (Equation 12) approaches one (1) in the limit that r_{xy} approaches zero. The other two terms will be for when x does not equal y, and the variables in the sine term come from Equation 14 and r_{xy}, which is the distance between the atoms in the molecule.

Acknowledgements

The authors would like to thank Drs. Doug Meier, Ian Anderson, Dale Newbury, and Gerry Danilatos for helpful discussions.

References

Belkorissat, R., Kadoun, A., Dupeyrat, M., Khelifa, B. & Mathieu, C., 2004. Direct Measurement of Electron Beam Scattering in the Low Vacuum SEM. Microchim. Acta 147, 135-139.

Bilde-Sorensen, J.B. and Appel, C., 1997. X-Ray Spectrometry in ESEM and LVSEM: Corrections for Beam Skirt Effects in: Tholen, A.R. (Ed.), Proc. SCANDEM-97. Svenskt Tryck I Goteborg AB, Sweeden.

Bolon, R.B., 1991. X-Ray Microanalysis in the ESEM in: Howitt, D.G. (Ed.), Microbeam Analysis. San Francisco Press, San Francisco, pp. 199-200.

Carlton, R.A., 1997. The Effect of Some Instrument Operating Conditions on the X-Ray Microanalysis of Particles in the Environmental Scanning Electron Microscope. Scanning 19, 85-91.

Danilatos, G.D., 1988. Foundations of Environmental Scanning Electron Microscopy. Adv. Electron. Elect. Phys. 71, 109-250.

Danilatos, G.D., 1990. Equations of Charge Distribution in the Environmental Scanning Electron Microscope (ESEM). Scanning Microscopy 4(4), 799-823.

Danilatos, G.D., 2009. Optimum Beam Transfer in the Environmental Scanning Electron Microscope. J. Microsc. 234(1), 26-37.

Danilatos, G.D., 2012. Velocity and ejector-jet assisted differential pumping: Novel design stages for environmental SEM. Micron 43, 600-611.

Danilatos, G., Rattenberger, J. & Dracopoulos, V., 2011. Beam transfer characteristics of a environmental SEM and a low vacuum SEM. J. Microsc. 242(2), 166-180.

Doehne, E., 1997. A New Correction Method for High-Resolution Energy Dispersive X-Ray Analyses in the Environmental Scanning Electron Microscope. Scanning 19, 75-78.

Gauvin, R., Griffin, B., Nockolds, C., Phillips, M. & Joy, D.C., 2002. A Method to Measure the Effective Gas Path Length in the Environmental or Variable Pressure Scanning Electron Microscope. Scanning 24, 171-174.

Griffin, B.J., 1992. Effects of Chamber Pressure and Accelerating Voltage on X-Ray Resolution in the ESEM in: Bailey, G.W., Bently, J., Small, J. (Eds.), Proc. 50th Annual Meeting of the Electron Microscopy Society of America. San Francisco Press Inc., San Francisco, pp. 1324-1325.

Griffin, B.J. and Suvorova, A., 2003. Charge-Related Problems Associated with X-ray Microanalysis in the Variable Pressure Scanning Electron Microscope at Low Pressures. Micro. Microanal. 9, 155-165.

Griffin, B.J. and Nockolds, C.E., 1996. Quantitative EDS Analysis in the Environmental Scanning Electron Microscope (ESEM) Using a Bremstrahlung Intensity-Based Correction for Primary Electron Beam Variation and Scatter in: Bailey, G.W., Corbett, J.M., Dimlich, R.V.M., Michael, J.R., Zaluzec, N.J. (Eds), Proceedings of Microscopy and Microanalysis 1996. San Francisco Press Inc., San Francisco, pp. 842-843.

He, J. & Joy, D.C., 2002. Measurement of Elastic Cross-Sections for Gases. Micro. Microanal. 8 (Suppl. 2), 1542-1543.

He, J. & Joy, D.C., 2003. Measurement of Total Gas Scattering Cross-Section. Scanning 25, 285-290.

Horsewell, A., Appel, C.C., and Bilde-Sorensen, J.B., 1996. 'Leaky Vacuum' SEM for Materials Scientists in: Bailey, G.W., Corbett, J.M., Dimlich, R.V.M., Michael, J.R., Zaluzec, N.J. (Eds), Proceedings of Microscopy and Microanalysis 1996. San Francisco Press Inc., San Francisco, pp. 846-847.

Kadoun, A., Belkorissat, R., Khelifa, B. & Mathieu, C., 2003. Comparative study of electron beam-gas interaction in an SEM operating at pressures up to 300 Pa. Vacuum 69, 537-543.

Khouchaf, L., Mathieu, C. & Kadoun, 2010. Electron microbeam changes under gaseous environment: CP-SEM case and microanalysis limits in: Mendez-Vilas, A. and Diaz, J. (Eds.), Microscopy: Science, Technology, Applications and Education. Formatex Research Center, Badajoz, Spain, pp. 1273-1279.

Mansfield, J.F., 2000. X-Ray Microanalysis in the Environmental SEM: A Challenge or a Contradiction? Mikrochim. Acta 132, 132-137.

Mansour, O., Aidaoui, K., Kadoun, A., Khouchaf, L. & Mathieu, C., 2010. Monte Carlo simulation of the electron beam scattering under gas mixtures environment in a HPSEM at low energy. Vacuum 84, 458-463.

Mathieu, C., Khouchaf, L. & Kadoun, A., 2007. Exploring the high Pressure SEM in: Mendez-Vilas, A. and Diaz, J. (Eds.), Microscopy: Science, Technology, Applications and Education. Formatex Research Center, Badajoz, Spain,, pp. 779-786.

Newbury, D.E., 2002. X-Ray Microanalysis in the Variable Pressure (Environmental) Scanning Electron Microscope. J. Res. Natal. Inst. Stand. Technol. 107, 567-603.

Rattenberger, J., Wagner, J., Schrottner, H., Mitsche, S., Zankel, A., 2009. A Method to Measure the Total Scattering Cross Section and Effective Beam Gas Path Length in a Low-Vacuum SEM. Scanning 31, 107-113.

Stowe, S.J. and Robinson, V.N.E., 1998. The Use of Helium Gas to Reduce Beam Scattering in High Vapor Pressure Scanning Electron Microscopy Applications. Scanning 20, 57-60.

Wight, S., Gillen, G., Herne, T., 1997. Development of Environmental Scanning Electron Microscopy Electron Beam Profile Imaging with Self-Assembled Monolayers and Secondary Ion Mass Spectroscopy. Scanning 19, 71-74.

Wight, S.A. and Zeissler, C.J., 2000. Direct Measurement of Electron Beam Scattering in the Environmental Scanning Electron Microscope Using Phosphor Imaging Plates. Scanning 22, 167-172.

Wight, S.A., 2001. Experimental Data and Model Simulations of Beam Spread in the Environment Scanning Electron Microscope. Scanning 23, 320-327.

Figure Captions

Figure 1: (a) This diagram presents an exploded view diagram of the construction of the dual Faraday cup. A graphite block with a hole drilled in the center is embedded in epoxy such that only the top surface is exposed. The center conductor of one shielded cable is connected to the graphite block. A 200 micrometer metal foil aperture is fixed with carbon paint over the hole in graphite block. Strips of double stick tape, a layer of Mylar and another layer of double stick tape are placed over top of the 200 micrometer aperture opening, and a hole is cut out of the tape that exposes the aperture. A disk of metal foil, with a hole to align with the 200 micrometer aperture, is attached to the tape. The center conductor of a second shielded cable is connected to the metal foil. Finally, the 5 micrometer platinum aperture is aligned over the center of the 200 micrometer aperture and then carbon painted in place; (b) a three dimensional perspective view of the assembled dual Faraday cup.

Figure 2: (a) A plot of average number of collisions per electron as a function of stagnation gas thickness (mm) for 133 Pa of air, water vapor, and argon at 20 kV accelerating voltage; (b) A plot of average number of collisions per electron as a function of beam gas path length (mm) for 27 Pa, 53 Pa, 80 Pa, 106 Pa, 133 Pa, 266 Pa, 399 Pa, 532 Pa, and 655 Pa (0.2 Torr, 0.4 Torr, 0.6 Torr, 0.8 Torr, 1.0 Torr, 2.0 Torr, 3.0 Torr, 4.0 Torr, and 5.0 Torr) of water vapor at 20 kV accelerating voltage.

Figure 3: A plot of the measured scattering cross section as a function of accelerating voltage (kV) for water vapor with error bars representing one standard deviation. The calculated total scattering cross sections using either the first or mean ionization potential are also plotted, corresponding to a minimum scattering angle (2.5×10^{-4} rad.) that matches the 5 μm dual Faraday cup and the 10mm working distance used for the measurement.

Figure 4: A plot of scattering cross section as a function of accelerating voltage (kV) for air with error bars representing one standard deviation. The calculated total scattering cross sections using either the first or mean ionization potential are also plotted, corresponding to a minimum scattering angle (2.5×10^{-4} rad.) that matches the 5 μm dual Faraday cup and the 10mm working distance used for the measurement.

Figure 5: A plot of scattering cross section as a function of accelerating voltage (kV) for argon with error bars representing one standard deviation. The calculated total scattering cross sections using either the first or mean ionization potential are also plotted, corresponding to a minimum scattering angle (2.5×10^{-4} rad.) that matches the 5 μm dual Faraday cup and the 10mm working distance used for the measurement.

Figure 6: A plot of the calculated scattering cross section as a function of accelerating voltage (kV) for water vapor for various minimum scattering angles. Effective aperture sizes are: 20 nm aperture; 5 μm aperture; 10 μm aperture; 20 μm aperture; and 200 μm aperture.

Table 1: Scattering cross sections and uncertainties for water, air, and argon that are plotted in Figures 5-7.

Table 2: Calculated fit parameters for the total scattering cross sections of water, air, and argon using the form $\sigma = A \cdot E^{-B}$, where A and B are constants, and E is the electron accelerating voltage in kV.

Highlights

- Scattering electrons out of the primary beam impacts quantitative chemical analysis
- Scattering cross sections measured with a dual Faraday cup device
- Measurements are compared with cross sections calculated from theory
- Agreement with other measurements; factor of 2 difference with theory

Table 1

E_0 (keV)	H_2O (m^2)	Unc (m^2)	Air (m^2)	Unc (m^2)	Argon (m^2)	Unc (m^2)
5	3.71e-21	0.08e-21	5.37e-21	0.19e-21	6.5e-21	0.4e-21
10	1.89e-21	0.03e-21	2.97e-21	0.03e-21	3.65e-21	0.05e-21
15	1.42e-21	0.02e-21	2.01e-21	0.02e-21	2.63e-21	0.03e-21
20	9.9e-22	0.2e-22	1.55e-21	0.02e-21	2.02e-21	0.02e-21
25	8.62e-22	0.19e-22	1.25e-21	0.019e-21	1.63e-21	0.02e-21
30	7.34e-22	0.19e-22	1.12e-21	0.012e-21	1.40e-21	0.019e-21

Table 2

	A (m^2/kV))	B
Water	1.57e-20	-0.905
Air	2.27e-20	-0.892
Argon	2.60e-20	-0.856

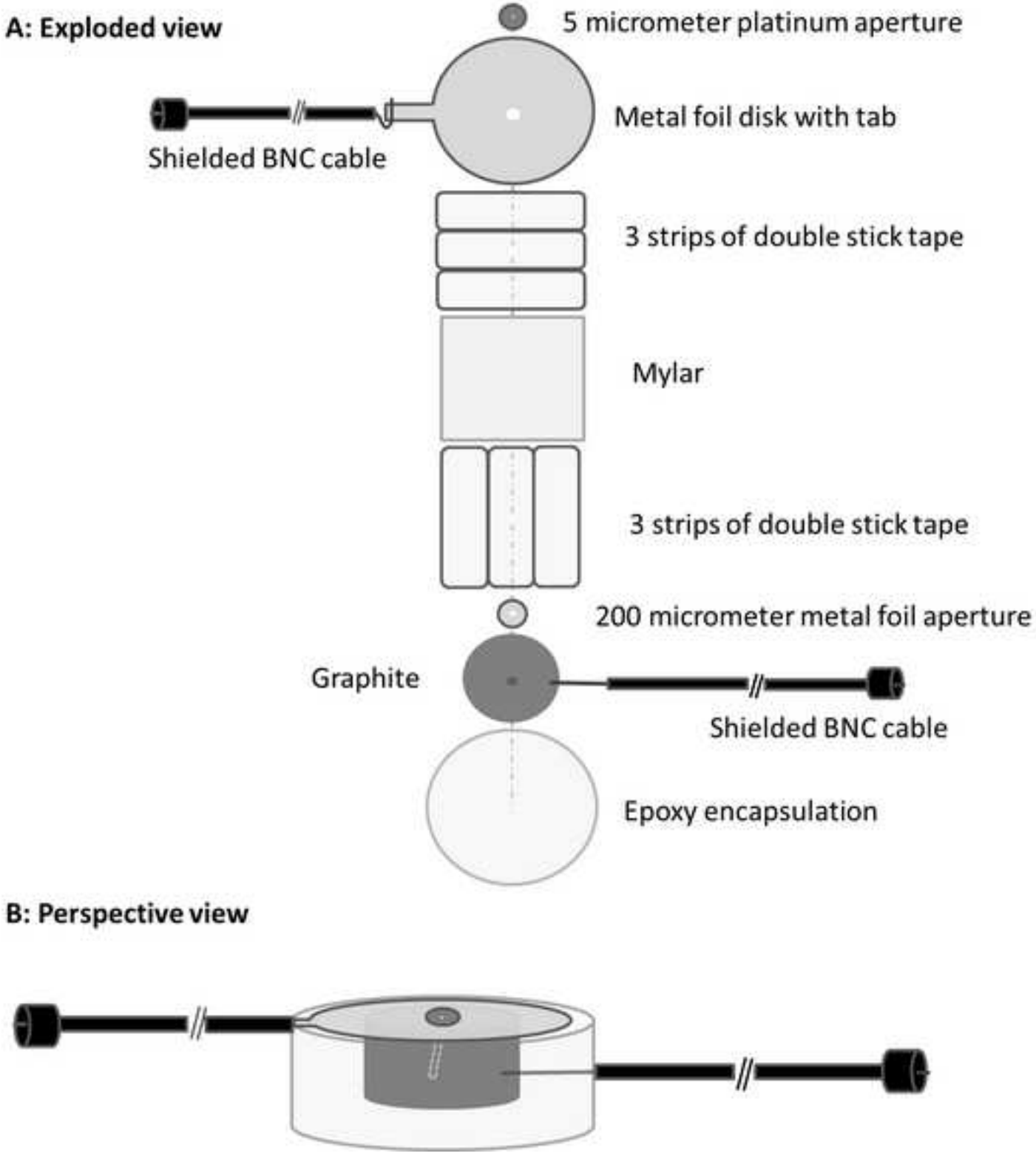

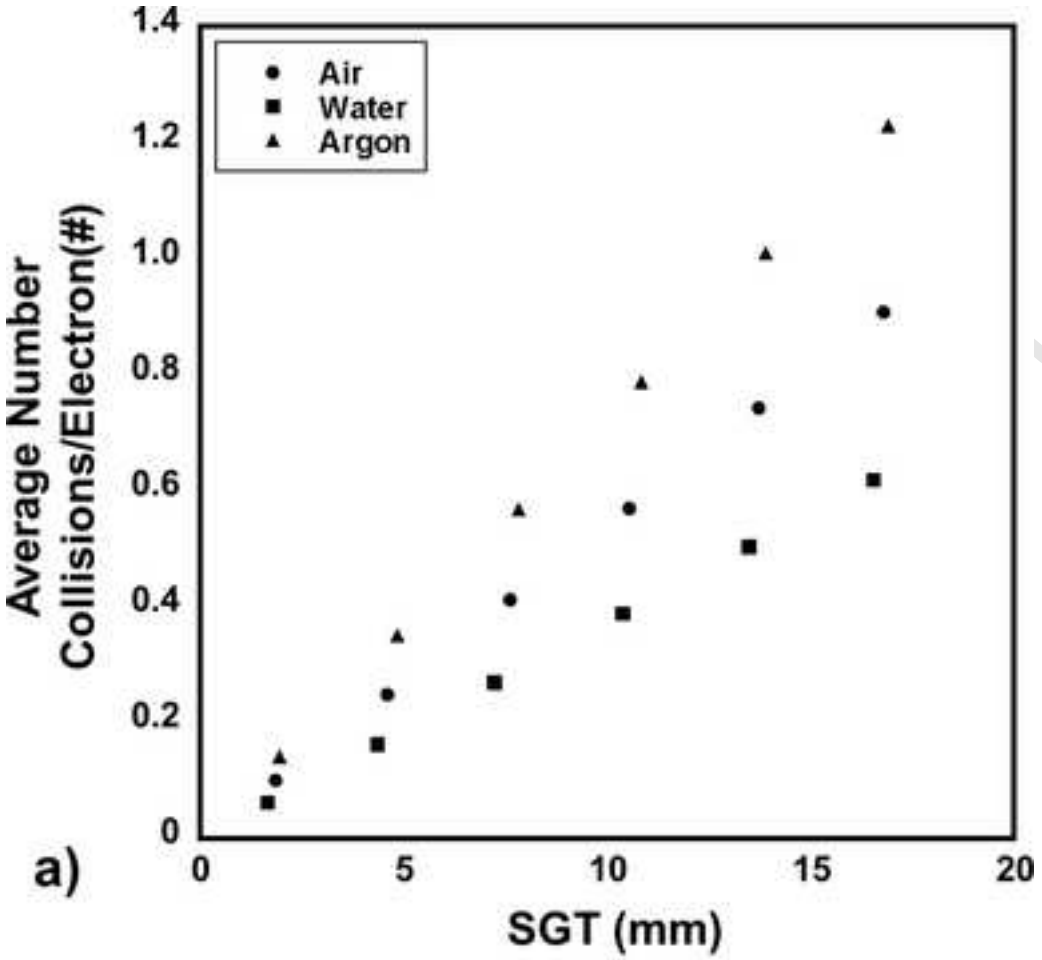

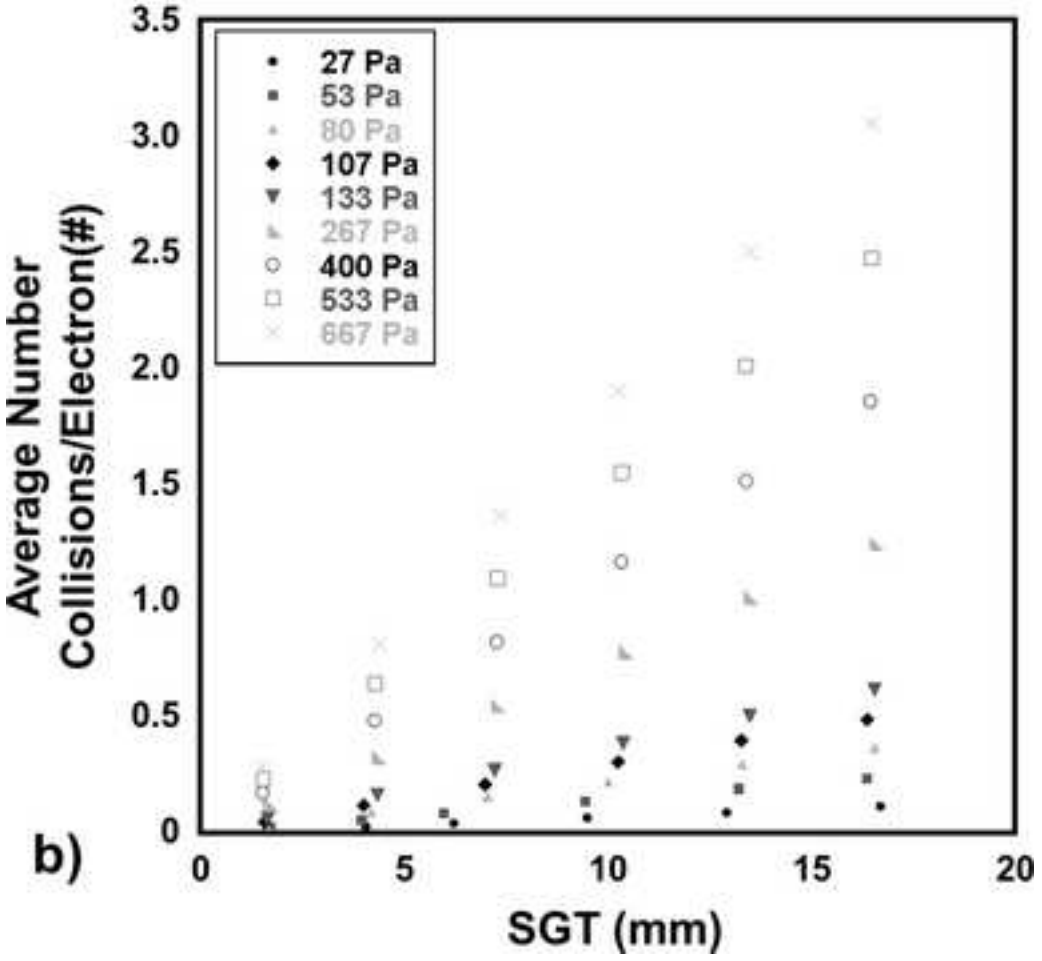

Figure 3

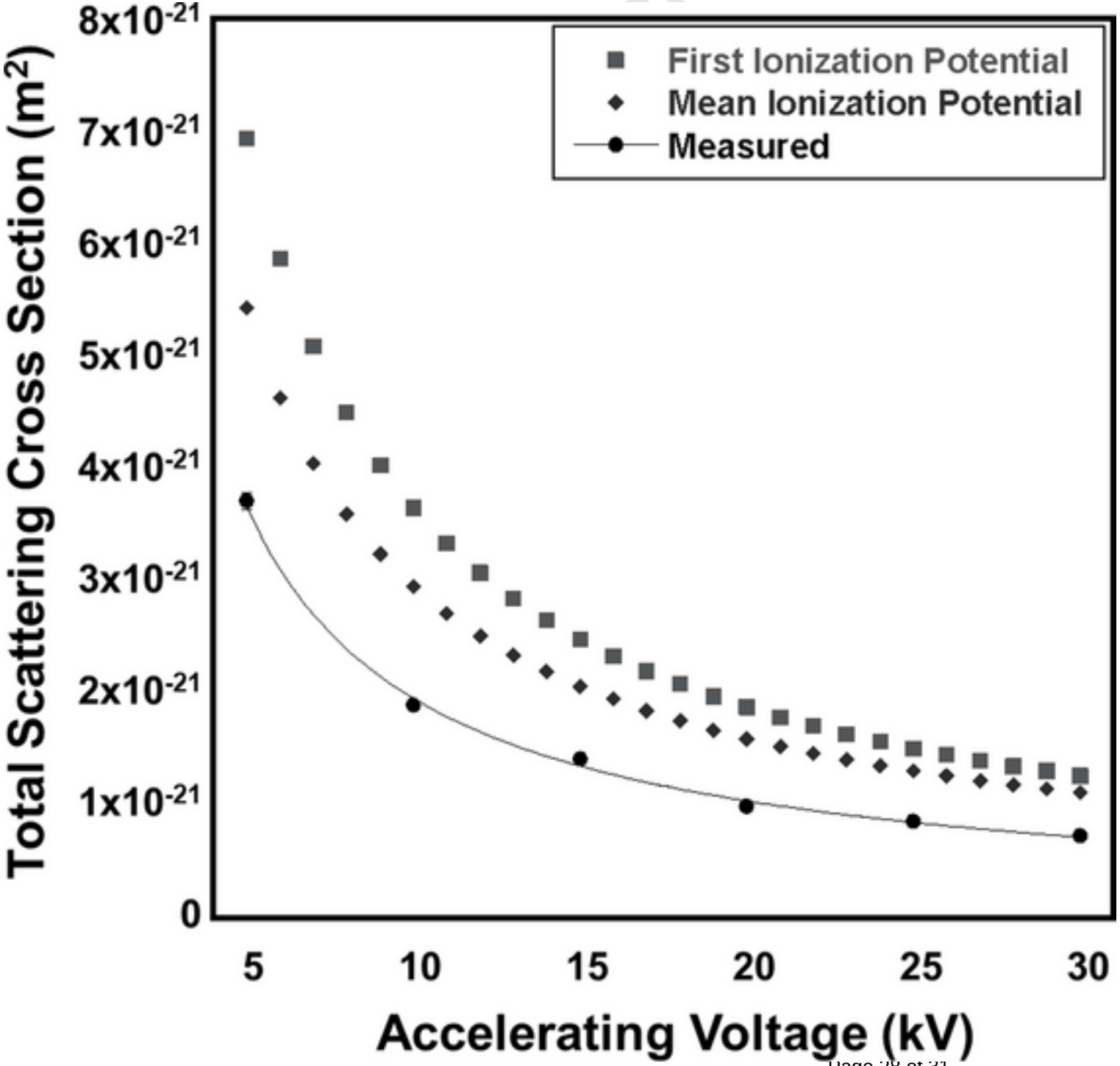
Total Scattering Cross Section (m²)
8x10-21
7x10-21
6x10-21
5x10-21
4x10-21
3x10-21
2x10-21
1x10-21
0
First Ionization Potential
Mean Ionization Potential
Measured
5
10
15
20
25
30
Accelerating Voltage (kV)

Figure 4

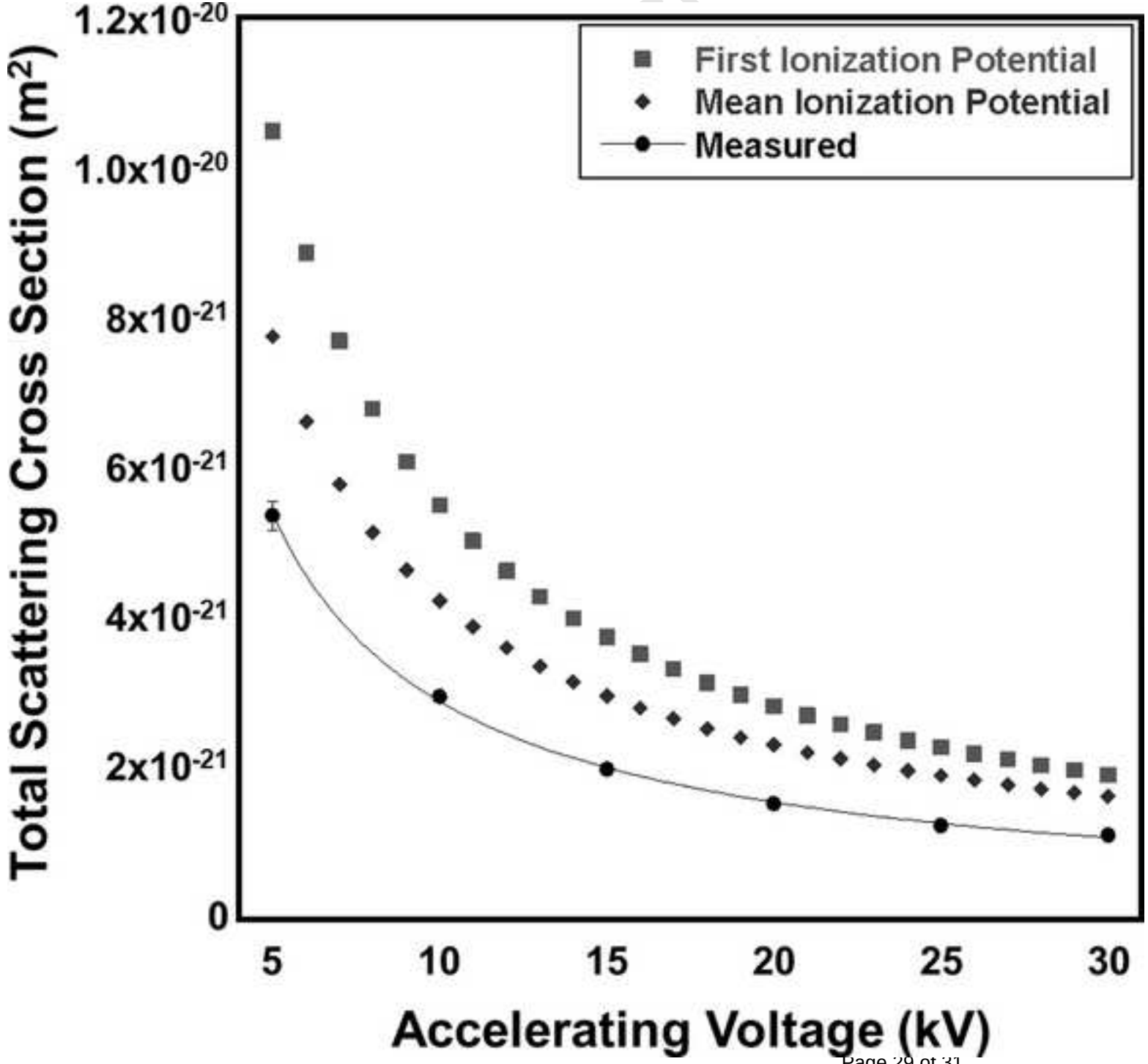
First Ionization Potential
Mean Ionization Potential
Measured
Total Scattering Cross Section (m²)
1.2x10-20
1.0x10-20
8x10-21
6x10-21
4x10-21
2x10-21
0
5
10
15
20
25
30
Accelerating Voltage (kV)

Figure 5

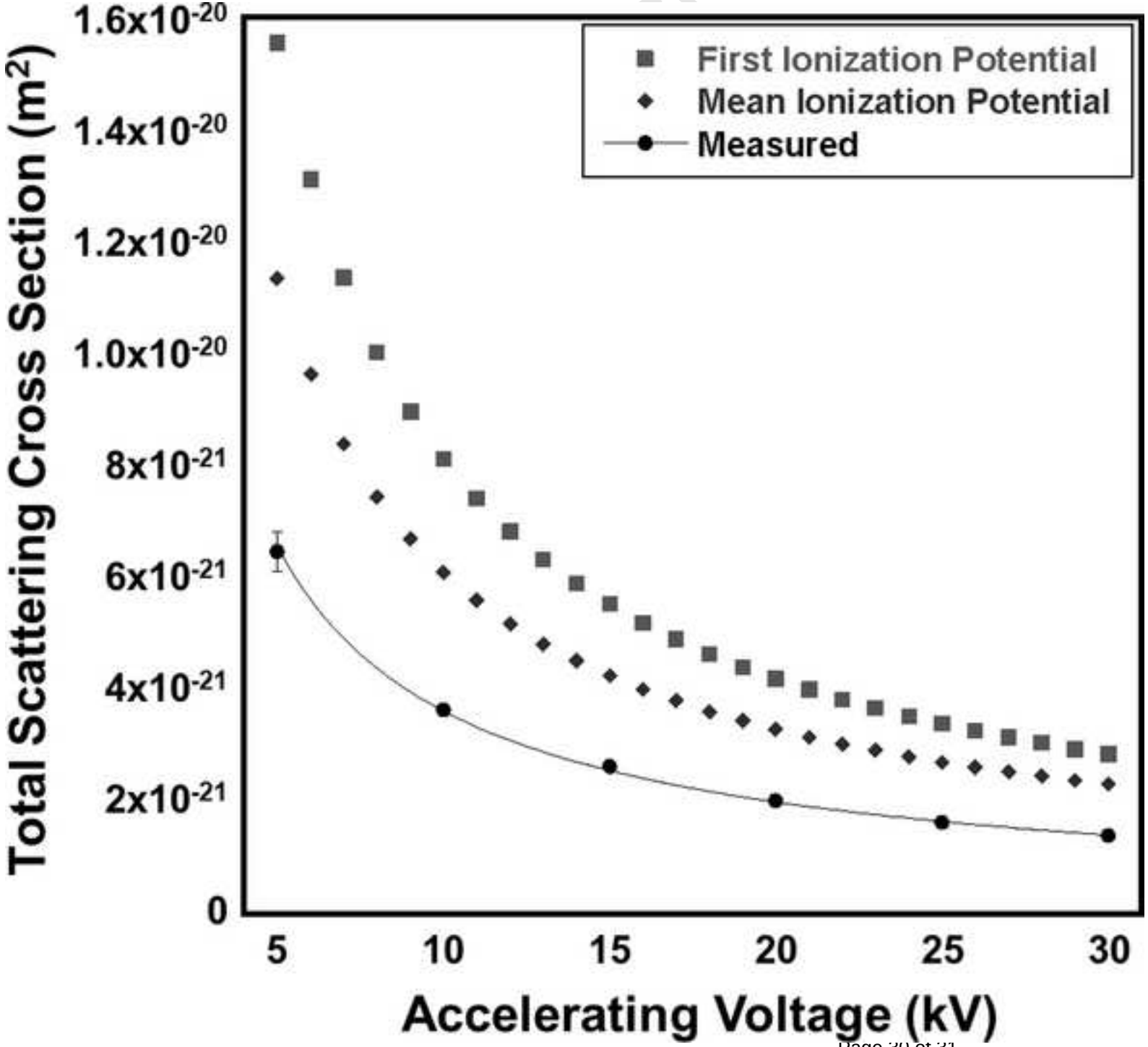
Total Scattering Cross Section (m²)
1.6x10-20
1.4x10-20
1.2x10-20
1.0x10-20
8x10-21
6x10-21
4x10-21
2x10-21
0
5
10
15
20
25
30
Accelerating Voltage (kV)
First Ionization Potential
Mean Ionization Potential
Measured

Figure 6

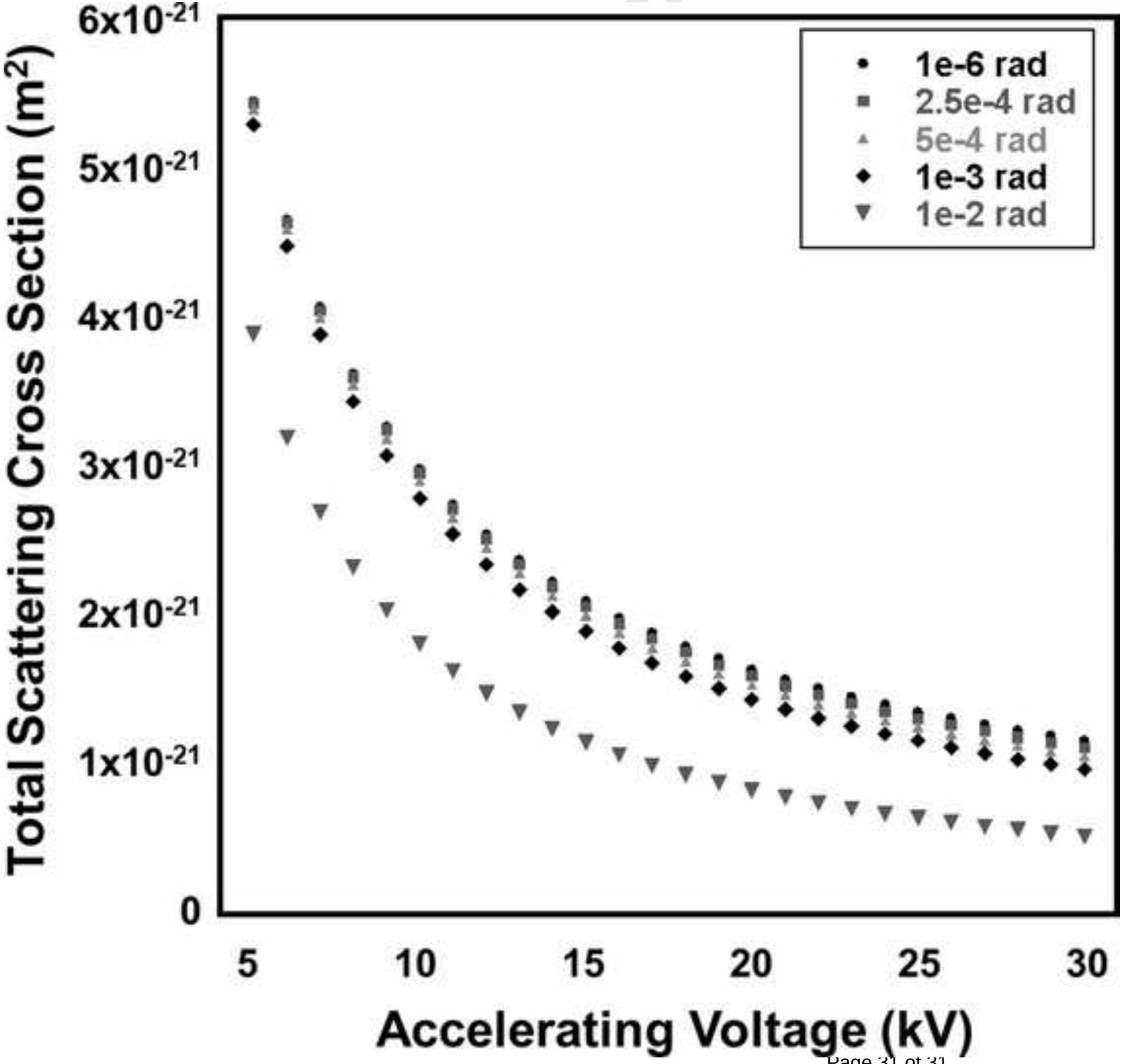
Total Scattering Cross Section (m²)
6x10-21
5x10-21
4x10-21
3x10-21
2x10-21
1x10-21
0
5
10
15
20
25
30
Accelerating Voltage (kV)
1e-6 rad
2.5e-4 rad
5e-4 rad
1e-3 rad
1e-2 rad